Model-independent measurements of bar pattern speeds

Joris Gerssen
Space Telescope Science Institute, 3700 San Martin Drive, Baltimore, MD 21218, USA

Konrad Kuijken
Sterrewacht Leiden, PO Box 9513, 2300 RA Leiden, The Netherlands

Michael R. Merrifield
School of Physics and Astronomy, University of Nottingham, Nottingham NG7 2RD

ABSTRACT

The pattern speed in one of the fundamental parameters that determines the structure of barred galaxies. This quantity is usually derived from indirect methods or by employing model assumptions. The number of bar pattern speeds derived using the model independent Tremaine & Weinberg technique is still very limited. We present the results of model independent measurements of the bar pattern speed in four galaxies ranging in Hubble type from SB0 to SBbc. Three of the four galaxies in our sample are consistent with bars being fast rotators. The lack of slow bars is consistent with previous observations and suggests that barred galaxies do not have centrally concentrated dark matter halos. This contradicts simulations of cosmological structure formation and observations of the central mass concentration in nonbarred galaxies.

Subject headings: galaxies: fundamental parameters — galaxies: kinematics and dynamics —

1. Introduction

The rate at which a bar rotates, the bar pattern speed, is one of the key parameters that controls the morphology and dynamical structure of a barred galaxy. Most determinations of the bar pattern speed rely on indirect methods such as identifying morphological features with resonance radii or by fitting models to observed velocity fields. A number of reviews describing these methods in detail can be found in the proceedings of 'Disks of Galaxies: Kinematics, Dynamics and Perturbations' (e.g. Teuben 2002). A more direct, non-model dependent method to estimate the bar pattern speed is due to Tremaine & Weinberg (1984, hereafter TW). Kent (1987) and Kent & Glaudell (1989) were the first to apply this method to stellar spectra. Merrifield & Kuijken (1995) observed the same galaxy, NGC 936, but used CCD spectroscopy to obtain spectra with signal-to-noise ratios. In subsequent years the TW method has been applied to a few more barred galaxies: NGC 4596 (Gerssen et al. 1999), NGC 1023 (Debattista & Williams 2001) and NGC 7079 (Debattista et al. 2002). Recently, Aguerri et al. (2003) presented an application of the the TW method to a sample of five SB0 galaxies.

Interestingly, the results obtained with the TW method suggest that the central regions in barred galaxies are not dominated by dark matter halos, unlike their unbarred counterparts. However, this could be a selection effect because the TW method is best suited to gas poor early type barred galaxies where the effects of dust extinction are minimised. Indirect techniques on the other hand usually rely on the presence of gas and are therefore restricted to later type barred galaxies. Neither the TW method nor the indirect techniques may therefore be representative of the whole population of barred galaxies.

The number of barred galaxies that have been observed to date using the TW method, mainly SB0 galaxies, is too small to unequivocally ascertain whether centrally concentrated dark matter halos are truly absent in barred galaxies. However, even SB0 galaxies are not completely devoid of dust. In the absence of any quantitative predictions of the effect of dust on TW measurements it may be unnecessarily restrictive to apply this method to SBO galaxies only. In this paper we present an analysis of the bar pattern speed in four barred galaxies using the TW method. Three galaxies, NGC 271, NGC 1358 and ESO 281-31 are early type barred galaxies. The fourth galaxy, NGC 3992, an SBbc type is of somewhat later type and was included to empirically assess how well the TW method can recover the pattern speed in such a system.

2. Tremaine & Weinberg method

Starting from the continuity equation TW showed that it is possible to derive an expression that directly relates the pattern speed Ω_p to two observationally accessible quantities: the luminosity weighted mean velocities and the luminosity weighted mean densities along lines parallel to disk major axis. The underlying assumption is therefore that the intensity is proportional to density. In reality the continuity equation is never strictly satisfied because of the continuous formation of stars. However, in regular, early type spiral galaxies this formation process is sufficiently slow that the TW method can be applied.

In its original form the method is sensitive to centering errors and suffers from low signal-to-noise ratios due to the — relative to the night sky — low surface brightness of galaxies. Merrifield & Kuijken (1995) used a revised implementation of the TW method that circumvents these two drawbacks. Briefly, this implementation requires the determination of the *mean* line-of-sight velocities and the *mean* positions of the stars along lines parallel to the barred galaxy's major axis. Merrifield & Kuijken realised that a luminosity-weighted mean velocity is naturally obtained by analysing the stellar absorption lines of a longslit spectrum summed along its spectral rows. Moreover, this procedure also significantly increases the signal-to-noise of the final spectrum. The intensity profile of the stars along a slit can be obtained by collapsing the spectrum along the wavelength direction. Both observables required by the TW method can therefore be obtained from the same data set. With this implementation of the TW method the pattern speed follows from the slope of a linear fit to the mean velocities and mean intensities of longslit spectra obtained parallel to the major axis of the disk.

$$\Omega_p \sin i = \frac{\langle X \rangle - X_0}{\langle V \rangle - V_0} \tag{1}$$

where X_0 is the luminosity center in the reference frame of the spectra and V_0 is the systemic velocity of the galaxy.

The required observations are essentially measurements of the deviation from symmetry. Galaxies with a bar major axis position angle in between about 20 to 70 degrees from the disk major and minor axis are therefore suitable for an application of the TW method. Although the TW signature will have its maximum strength when this angle is close to 45 degrees.

3. Observations and Reduction

Longslit stellar absorption line spectra centered around the Mg b triplet near 5200 Å and with a spectral resolution of $\sim$ 5000 were obtained for four barred galaxies. Three galaxies, NGC 271, NGC 1358 and ESO 281-31, were observed from La Silla on the nights of August 28 and 29 2000 using the longslit spectroscopic mode of the ESO Multi-Mode Instrument (EMMI) on the New Technology Telescope (NTT). A fourth galaxy, NGC 3992, was observed from La Palma on the night of January 30 2000 using the blue arm of the ISIS spectrograph on the William Herschel Telescope (WHT). Both combinations of telescope and spectrograph have rather similar characteristics in terms of overall efficiency and dispersion per pixel. Specifically, for the NTT data the dispersion per pixel is 17.3 $\mathrm{km\,s^{-1}}$ and the pixel scale is 0.54 arcsec, for the WHT data the numbers are 13.3 $\mathrm{km\,s^{-1}}$ and 0.8 arcsec respectively. The data for all four galaxies are therefore of comparable quality.

The galaxies and their relevant properties are listed in table 1. Position angles were derived from an isophotal analysis of Digital Sky Survey images using the task ELLIPSE in IRAF. Contour plots of the four galaxies with the positions of the slit overlaid are shown in fig 1. The slits were positioned parallel to the disk major axis of each galaxy and centered on either the nucleus or toward the bar edges. In two cases (NGC 3992 and ESO 281-31) we also obtained

spectra along positions intermediate between the center and the end of the bar. A complete log of the observations is given in table 2.

All spectra were reduced in IRAF. The exposures were bias subtracted and flatfielded. Small corrections for vignetting near the slit-ends were also applied. However, in practice the target galaxies were all significantly smaller than the slit length. The spectra were wavelength calibrated and binned onto a logarithmic wavelength scale using arclamp calibration frames taken before or after each science exposure. If necessary, contaminating light of foreground stars was removed by linearly interpolating over these stars. The sky background was subtracted using the rows near the ends of the slit. Finally, all rows in single longslit spectrum were summed to a one-dimensional array excluding the outer most rows. After sky subtraction the rows toward the ends of the slit contain only noise. Including these rows lowers the signal-to-noise of the summed spectrum to a point were no meaningful velocity analysis can be performed.

Stellar template spectra were also obtained on both observing runs. Spectra of the K0III stars HD210396 and HD168424 were obtained on the NTT. On the WHT run spectra were taken of the template star HD107288 (K0).

4. Velocity Analysis

Stellar velocities were derived using the standard assumption that the observed galaxy spectrum is the convolution of a typical stellar template spectrum (usually a K giant) with the line-of-sight velocity distributions (LOSVD). Several techniques have been developed over the years to obtain the LOSVDs from galactic spectra. The standard cross correlation technique (Tonry & Davis, 1979) is among the most widely used such methods but assumes that LOSVD can be approximated by a Gaussian. We used an updated version of this method, the IRAF task XCSAO (see Kurtz & Mink 1998) to obtain estimates of the mean velocities in the galaxies. The continuum subtracted galactic spectra where correlated against all continuum subtracted template spectra that were available for each run. The results, however, do not depend significantly on the choice of template. Before cross-correlating the spectra, the data were Fourier filtered to suppress noise (large k numbers) and residual continuum variations (low k numbers).

An initial TW analysis of the spectra was also performed using XCSAO. However, the distribution of stellar velocities in a disk galaxy often deviates from a Gaussian distribution. Especially in the tangential direction, and the tangential velocity component dominates the line-of-sight velocities along the major axis of a disk galaxy.

A more refined analysis was subsequently performed using the Unresolved Gaussian Decomposition (UGD) method of Kuijken & Merrifield (1993). UGD can measure deviations from Gaussian profiles by assuming that the intrinsic line profile shape can be approximated as a sum of Gaussians spaced at regular (user-defined) intervals. The only free parameters in the fit are the amplitudes of the individual Gaussian components. The advantages of a non-parametric method like UGD are that it does not presuppose a particular form for the LOSVD, and that it returns well-defined errors. Following Merrifield & Kuijken (1995) we fit the LOSVD of each spectrum

with three Gaussian components uniformly placed at $V_{\rm sys} - 1.5\sigma_{\rm est}$, $V_{\rm sys}$ and $V_{\rm sys} + 1.5\sigma_{\rm est}$. (Merrifield & Kuijken using data with higher signal-to-noise ratios were able to fit two additional components at -3σ and 3σ respectively.) The systemic velocities $V_{\rm sys}$ as well as the estimates of the velocity dispersions were obtained from the cross-correlation analysis. Although weakly, the derived LOSVDs do indeed show the expected asymmetries (e.g. Merrifield & Kuijken 1995). The estimates of the pattern speed obtained with UGD are therefore not significantly different from the XCSAO analysis. For data of higher signal-to-noise ratios these differences would be more pronounced. Besides a providing consistency check, the main advantage of analysing the spectra with the UGD method is the robust estimate of the errors.

5. Results

Along each slit the luminosity weighted mean velocity and the mean light distributions were derived in the manner outlined above. The results are shown for all four galaxies in fig 2. The errors in the intensity weighted mean positions along the slit are negligible compared to the velocity errors and have therefore been ignored in the analysis. The derived velocities were not corrected to heliocentric velocities since this is not required by the TW method. Nevertheless the velocities are close to the published systemic velocities with the exception of ESO 281-31. The literature value (see table 1) for this galaxy differs by some $1500\,{\rm km\,s^{-1}}$ from the value derived here. The published redshift is probably in error since the NED database does not give a reference but simply states that the redshift was derived prior to 1992.

The reliability of the velocity errors returned by the UGD algorithm was assessed using a large set of artificially broadened, and noise added template spectra . The scatter in the mean velocities derived from the broadened template spectra was found to be comparable to the estimated velocity uncertainties. The slope of the linear fits to the mean velocities and the mean positions in each panel of fig 2 yields $\Omega_p \sin i$ for each galaxy. The best-fit values and their 1σ errors are listed in table 3.

Multiple exposures per slit were obtained for all slits positioned offset from the major axis. These offsets were commanded to the telescope by hand. The spatial coincidence of multiple exposures that were not obtained in sequence is therefore not perfect. To test whether this affects the derived pattern speeds we also derived the mean velocities and mean intensities in each individual slit. The dashed lines in fig 2 show the linear fits to the individual points (not shown to avoid crowding). The derived slopes are not significantly different from the values derived from the combined spectra.

5.1. NGC 271

The data of this galaxy are consistent with a well-defined pattern speed in this galaxy.

5.2. NGC 1358

Longslit spectra are available for the nucleus and on one side of the bar. Unfortunately, spectra on the opposite end of the bar could not be obtained. The pattern speed in this galaxy was derived using the individual exposures only. The low number of data points did not warrant an analysis on the combined spectra. Consequently, the derivation of the pattern speed is less secure in this galaxy than it is for the other galaxies in the sample.

5.3. ESO 281-31

More longslit spectra have been obtained for this galaxy than for the other galaxies observed with the NTT to facilitate a detailed comparison with the stellar kinematics derived from a complete Fabry-Perot data set in a forthcoming study. The longslit data are consistent with a well-defined pattern speed in this galaxy.

5.4. NGC 3992

The gas rich SBbc galaxy NGC 3992 has the latest Hubble type of all galaxies in this sample. The star formation rate in this system will therefore be higher than in the other three galaxies (e.g. Kennicutt 1998). The basic assumption of the TW method is that the number of tracers (i.e. stars) remains constant. This condition is least well satisfied in the case of NGC 3992. Indeed, the scatter in the points around the linear fit is larger than for any of the other — earlier type — galaxies in this sample. Several indirect studies of the pattern speed in NGC 3992 have been attempted based on modeling the gas kinematics. Hunter et al. (1988) find a value for the pattern speed in NGC 3992 of about 50 $\mathrm{km\,s^{-1}\,kpc^{-1}}$ and Kaufmann & Contopoulos (1996) derive a comparable value of 43.6 $\mathrm{km\,s^{-1}\,kpc^{-1}}$. Using their adopted distance of 14.2 Mpc we derive a pattern speed with the TW method that is considerably larger at $83 \pm 5\,\mathrm{km\,s^{-1}\,kpc^{-1}}$.

6. Co-rotation Radii and Bar Lengths

A consistency check on the numerical values of the pattern speed can be obtained by deriving the co-rotation radius in each galaxy, i.e. the radius where the stars rotate with the same angular frequency as the bar. Self-consistent bars cannot extent beyond their own co-rotation radius and, consequently, the ratio, $\mathcal{R}$, of the co-rotation radius to bar length cannot be smaller than 1.0. The circular velocities as a function of radius are required in order to derive the co-rotation radius. Unfortunately, published rotation curves are only available for the gas-rich system NGC 3992. Bottema & Verheijen (2002) have published an HI rotation curve for this system. However, this rotation curve is only available for radii beyond the bar. We therefore extrapolated the rotation curve inward assuming a constant value of $216\,\mathrm{km\,s^{-1}}$ (the average value obtained from their table 3). No rotation curves have been published for the other galaxies in the sample. Global HI

profiles are available for NGC 271 and NGC 1358 (Theureau et al. 1998) and can in principle be used to estimate the circular velocities, assuming the rotation curve at large radii is flat.

The global HI profiles are rather noisy and we have therefore attempted to measure the circular velocities directly from the stellar absorption line spectra. Although, these spectra were never intended to derive spatially resolved kinematics, a cross-correlation analysis (again using XCSAO) of the major axis spectra with the stellar template spectra still yields meaningful estimates of the mean stellar velocities as a function of radius, see fig 3. The derived mean stellar velocities are constant at large radii. However, the amplitude of the flat part is somewhat lower than the circular velocity. This difference, the asymmetric drift, is accounted for by the stellar velocity dispersion. Our major axis spectra are of sufficient quality to measure the central velocity dispersions, σ_0, of each galaxy in our sample. The central dispersions are obtained from the Gaussian velocity distribution that, convolved with a stellar template spectrum, gives the best match to the central row of each longslit galaxy spectrum. The radial behaviour of the velocity dispersion cannot be ascertained from these spectra. Instead we assume that the dispersions decline as $\sigma = \sigma_0 \exp(-R/2h)$, where h is the photometrical scale length. An estimate of h is obtained from the same photometry used to determine the bar length (see section 6.1) by measuring the slope of the azimuthally averaged radial surface brightness profile outside the bulge region. The best-fit values of σ_0 and h are listed in table 3.

With the above assumption for the radial behaviour of the velocity dispersion and by assuming that the circular velocity is flat at large radii the asymmetric drift can be calculated as follows (e.g. Gerssen et al. 2000)

$$V_{\rm circ}^2 - V_{\rm star}^2 = \sigma_R^2 \left[\frac{2R}{h} - \frac{1}{2} \right], \tag{2}$$

where σ_R is the radial component of the velocity dispersion. However, from our observations we only have an estimate of the line-of-sight velocity dispersions. Rather than invoking additional assumptions about the distribution of the velocity dispersion components we identify σ_R with the observed dispersions and recognize that this approach yields an upper limit to the asymmetric drift correction. Using this approach we find that near the co-rotation radii the asymmetric drift corrections are $\sim 10\,{\rm km\,s^{-1}}$ for both NGC 1358 and ESO 281-31 and $\sim 30\,{\rm km\,s^{-1}}$ for NGC 271. Although not negligible, the upper limits to the asymmetric drift corrections make only a small change to the derived co-rotation radii. These radii and their uncertainties are listed in table 3.

6.1. Bar lengths

The other piece of information required to derive the ratio $\mathcal{R}$ is the length of the bar. To this end we obtained photometry for each of the four galaxies in the sample from several sources. K-band photometry for NGC 271 was obtained from the Two Micron All Sky Survey (2mass). An I-band image of NGC 1358 was obtained from from the Isaac Newton Group (ING) archive. I-band images of ESO 281-31 and NGC 3992 were kindly made available by Victor Debattista and Roelof Bottema respectively.

Estimates of the bar semi-major axis length in each galaxy were derived analogous to Aguerri

et al. (2003). With one exception the techniques they use are based on Fourier decompositions of the deprojected azimuthal surface brightness profiles. The first estimate of the bar length exploits the fact that along a bar the phase of the $m = 2$ component of a Fourier decomposition is constant (Debattista & Sellwood, 2000). The bar length can thus be determined from a plot of these phases as a function of radius. The second method is based on the ratio of the intensities in the bar and interbar regions (Aguerri et al. 2000). The bar and interbar intensities are defined as linear combinations of the $m = 0, 2, 4$ and 6 terms of the Fourier decomposition: $I_b = I_0 + I_2 + I_4 + I_6$ and $I_{ib} = I_0 - I_2 - I_4 + I_6$. Within the bar the ratio of the bar and interbar intensities should be larger than $0.5[\max(I_b/I_{ib}) - \min(I_b/I_{ib})] + \min(I_b/I_{ib})$. The left panels of fig 4 show the results of the two methods applied to the surface photometry of ESO 281-31. With these data it also proved possible to obtain the bar length from a bulge, disk and bar component fit to the surface brightness profile along the bar major axis. Both the bulge and the disk were assumed to be exponential and the bar was parametrised by the flat-type profile of Prieto et al. (2001). The bar lengths estimated with the three different method are similar to within one arcsec (fig 4).

The photometry available for the other three galaxies is of somewhat lower quality and the bar length analysis in these galaxies was therefore restricted to the Fourier decomposition methods only, fig 5. The adopted bar length for each galaxy listed in table 3 is the average of the different methods used to estimate this length. In general, the different estimates agree quite well and the associated errors are therefore small. Only for NGC 3992 does the difference appear to be rather large. The estimate based on the ratio I_b/I_{ib} is comparable to the bar length given by Bottema & Verheijen (2002). However, the estimate based on the phase of the $m = 2$ component yields a considerably smaller bar length in this galaxy. The surface brightness profile along the bar in NGC 3992 shows a clear break at a radius that coincides with the smaller of the two estimates. Perhaps the region between the break in the intensity profile and the beginning of the spiral arm structure (which coincides with the larger of the two estimates) is a region of gradual transition from bar orbits to disk orbits. Simulations show that such regions are populated with chaotic orbits that can appear to either support bar structure or spiral structure (Kaufmann & Contopoulos 1996).

6.2. Bar lengths 2: an alternative method

The galaxies in our sample were all selected on the grounds of having clearly identifiable bars in optical images. A more quantitative evaluation of the bar strength was made using the bar strength analysis technique of Abraham & Merrifield (2000). This analysis shows that the bars in our sample are all of comparable strength. There is no hint of a correlation between the bar strength and the bar pattern speed. Kormendy (1979) suggested that bars slow down as they become weaker. The distribution of barred galaxies with measured pattern speeds in Hubble Space (Merrifield 2002) is also not inconsistent with this explanation. However, the presently available data does not support this interpretation, but the range in bar strengths covered is still small. Aguerri et al. (2003), using literature classifications for the strength of the bars in their sample, reach a similar conclusion. Incidentally, the bar strength analysis provides an additional estimate

of the bar semi major axis length (listed in the last column of table 3). All derived bar lengths are consistent with the results presented in section 6.1.

7. Discussion

Once the the co-rotation radii and the bar lengths have been derived it is trivial to determine the ratio $\mathcal{R}$. The numerical values for all four galaxies are given in table 4. Ratios of $\mathcal{R}$ smaller than 1.0 are unphysical because they violate self-consistency. However, there is no a priori reason for the ratios not to be significantly larger than 1.0. N-body simulations of barred galaxies (Debattista & Sellwood 2000) as well as analytical arguments (Weinberg 1985) suggest that the rate at which bars rotate is rapidly (i.e. within a few orbital periods) slowed down due to the dynamical friction exerted by the dark halo on the bar. Bars with a ratio $\mathcal{R}$ of $\gtrsim 1.0$ are close to rotating as fast as they physically can and are therefore said to be "fast rotators". Bars with larger values of $\mathcal{R}$ are called slow bars. A somewhat arbitrary, but now commonly employed practise in the literature is to set the devision between fast and slow bars at a $\mathcal{R}$ ratio of about 1.4 to 1.5. Note that this does not imply anything about the absolute value of the pattern speed of a bar. To illustrate this point the derived pattern speeds are converted to physical units (column 3 of table 4) by assuming the distances (using an H_0 of $65\,\mathrm{km\,s^{-1}}$) and inclinations listed in table 1. These physical values show no correlation with $\mathcal{R}$ but three out of the four galaxies have pattern speeds that are consistent with fast rotators. Although the errors on $\mathcal{R}$ are skewed toward large values, the maximum likelihood values of $\mathcal{R}$ are clearly consistent with fast rotators for these three galaxies. The fourth galaxy, ESO 281-31, is only just consistent with a fast rotator. This system therefore warrants a more detailed study to confirm whether the bar in this galaxy is a genuine slow rotator.

The results obtained from this sample of four galaxies agree well with the previous determinations of bar pattern speeds using the TW method. These studies all find that bars rotate fast. The earlier studies, however, were limited to the earliest type barred galaxies, SB0 and SBa type galaxies. A Compilation (Elmegreen et al. 1996) of indirect results obtained for later type barred galaxies corroborates the TW results. The average bar pattern speed obtained from this compilation is $\langle\mathcal{R}\rangle = 1.2 \pm 0.2$. A direct conformation of the results relies on a successful application of the TW method to later type barred galaxies. The gas-rich system NGC 3992 was specifically included in the sample presented here to test the feasibility of such an application. The derived $\mathcal{R}$ ratio for this system is formally consistent with a self-consistent bar. Although the scatter in the derived velocities (fig. 2) and the difference between the TW derived pattern speed and the published — indirect — values suggests that this agreement is perhaps fortuitous. However, Aguerri et al. (2003), find that two of the five SB0 galaxies in their sample also have a $\mathcal{R}$ ratio smaller than 1.0 but argue that this just reflects the scatter due to the uncertainties in the position angles of the bar and of the disk. Such uncertainties can lead to either over- or underestimates of the derived pattern speed as simulations by Debattista (2003) have shown.

An alternative explanation for the the small $\mathcal{R}$ value in NGC 3992 is that it is due to dust absorption. Intervening dust will affect the derivation of the luminosity weighted mean velocities

and intensities. The derived pattern speed can therefore be quite different from its intrinsic value. This problem can be circumvented observationally by using near IR observations since they are less affected by dust obscuration. The CO bandhead at 2.3μ proofed to be well suited to derive stellar kinematics and could therefore be used for a TW type analysis in the near IR. Baker et al. (2001) attempted to do just that for NGC 1068 but found a ratio much smaller than 1.0. However, they only obtained two slit positions, which makes it hard to constrain the pattern speed adequately.

The result obtained for the Sbc galaxy NGC 3992 is consistent with the results obtained for SB0 systems (e.g. Aguerri et al 2003). A definitive test of whether the TW method is applicable to later type — gas rich — barred galaxies therefore remains to be done. But with the current availability of longslit near-IR spectrographs such a test is now feasible. The consensus reached from the studies of early type barred galaxies, is that all bars appear to be fast rotators. The dynamical friction between the bar and the dark matter halo must therefore be small and this implies that barred galaxies do not have centrally concentrated dark matter halos. Navarro, Frenk & White (1997) show from cosmological simulations that galaxies should have a universal dark matter halo distribution that is peaked in the center. Indeed, (Courteau & Rix 1999) find that nonbarred galaxies are strongly dark matter dominated in their centers. The results for barred galaxies therefore appear to be at odds with their nonbarred counterparts (e.g. Sellwood 2000). Whether these results hold up for later type barred galaxies depends largely on how well the TW method can be applied to near-IR spectra. An additional use of a large sample of barred galaxies with measured kinematics is to test whether these galaxies follow the Tully-Fisher relation (Courteau et al. 2003). This relation is based mostly on observations of nonbarred galaxies, and can for these systems be explained in terms of the CDM paradigm.

Based on observations collected with the NTT at the European Southern Observatory of La Silla. The WHT is operated on the island of La Palma by the Isaac Newton Group in the Spanish Observatorio del Roque de los Muchachos of the Instituto de Astrofísica de Canarias. JG thanks Roeland van der Marel, Victor Debattista and Roelof Bottema for comments and discussions. Much of the analysis in this paper was performed using IRAF, which is distributed by NOAO.

REFERENCES

Abraham R. G., Merrifield M. R., 2000, AJ, 120, 2835

Aguerri J. A. L., Munoz-Tunon C., Varela A. M., Prieto M., 2000, A&A, 361, 849

Aguerri J. A. L., Debattista V. P., Corsini E. M., 2003, MNRAS, 338, 465

Baker A. J., Schinnerer E., Scoville N. Z., Englmaier P. P., Taconni L. J., Taconni-German L. E., Thatte N., 2001 in, Knapen J. H, Beckman J. E., Shlosman I., Mahoney T. J, eds, ASP Conf. Ser. Vol. 249, The central kiloparsec of starbursts and AGN: the La Palma connection. Astron. Soc. Pac., San Fransisco, p. 78

Bottema R., Verheijen M. A. W., 2002, A&A, 388 ,793

Courteau S., Rix H-W., 1999, ApJ, 513, 561

Courteau S., Andersen D. R., Bershady M. A., MacArthur L. A., Rix H-W., 2003, ApJ (astro-ph/0305521)

Debattista V. P., Sellwood J. A., 2000, ApJ, 543, 704

Debattista V. P., Williams T. B., 2001, in, Funes J. G., Corsini E. M., eds, ASP Conf. Ser. Vol. 230, Galaxy Disks and Disk Galaxies. Astron. Soc. Pac., San Fransisco, p. 55

Debattista V. P., Corsini E. M. Aguerri J. A. L., 2002, MNRAS, 332, 65

Debattista V. P., 2003, MNRAS, 342, 1194

Elmegreen B. G., Elmegreen D. M., Chromey F. R., Hasselbacher D. A., Bissell B. A., 1996, AJ, 111, 2233

Gerssen J., Kuijken K., Merrifield M. R., 1999, MNRAS, 306, 926

Gerssen J., Kuijken K., Merrifield M. R., 2000, MNRAS, 317, 545

Hunter J. H., England M. N., Gottesman S. T., Ball R., Huntley J. M., 1988 ApJ, 324, 721

Kaufmann D. E., Contopoulos G., 1996, A&A, 309, 381

Kent S. M., 1987, AJ, 93, 1062

Kent S. M. laudell G., 1989, AJ 98, 1588,

Kennicutt R. C., 1998, ARA&A, 36, 189

Kormendy J., 1979, ApJ, 227, 714

Kuijken K., Merrifield M., R. 1993, MNRAS, 264, 712

Kurtz M .J., Mink D. J., 1998, PASP, 110, 934

Merrifield M. R., Kuijken K., 1995, MNRAS, 274, 933

Merrifield M. R., 2002, in, Athanassoula E., Bosma A. Mujica R. eds, ASP Conf. Ser. Vol. 275, Disks of Galaxies: Kinematics, Dynamics and Perturbations. Astron. Soc. Pac., San Fransisco, p. 175

Navarro J. F., Frenk C. S., White S. D. M., 1997, ApJ, 490, 493

Prieto M., Aguerri J. A. L., Varela A. M., Munoz-Tunon, C., 2001, A&A, 367, 405

Sellwood J. A., 2000, in, Dynamics of Galaxies: from the Early Universe to the Present, ASP Conference Series, Vol. 197, eds. F. Combes, G. A. Mamon, V. Charmandaris, p. 3.

Theureau G., Bottinelli L., Coudreau-Durand N., Gouguenheim L., Hallet N., Loulergue M., Paturel G., Teerikorpi P., 1998, A&AS, 130, 333

Tonry J., Davis M., 1979, AJ, 84, 1511

Tremaine S., Weinberg M. D., 1984, ApJ, 282, L5 (TW)

Teuben P. J., 2002, in, Athanassoula E., Bosma A. Mujica R. eds, ASP Conf. Ser. Vol. 275, Disks of Galaxies: Kinematics, Dynamics and Perturbations. Astron. Soc. Pac., San Fransisco, p. 217

Weinberg M. D., 1985, MNRAS, 213, 451

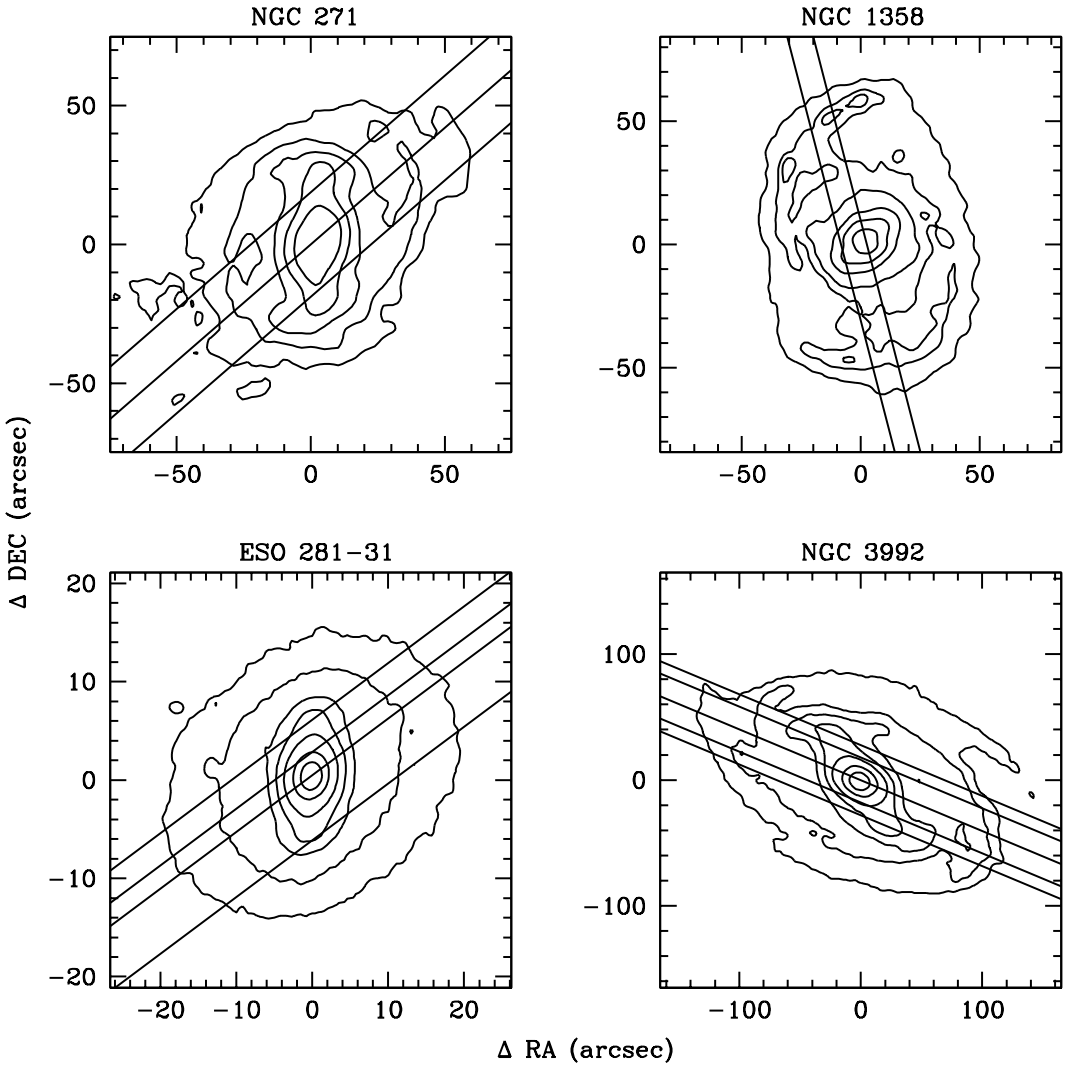

Fig. 1.— Contour plots of the four galaxies in the sample. Foreground stars present in the images were removed. North is to the top and east is to the left in each panel. The isocontours are chosen such as to best delineate the orientation of the bar and the disk. In all four galaxies the position angle of the bar is intermediate between the disk major and minor axis, as required by the TW method. The solid lines indicate the positions along which we obtained the stellar absorption line spectra.

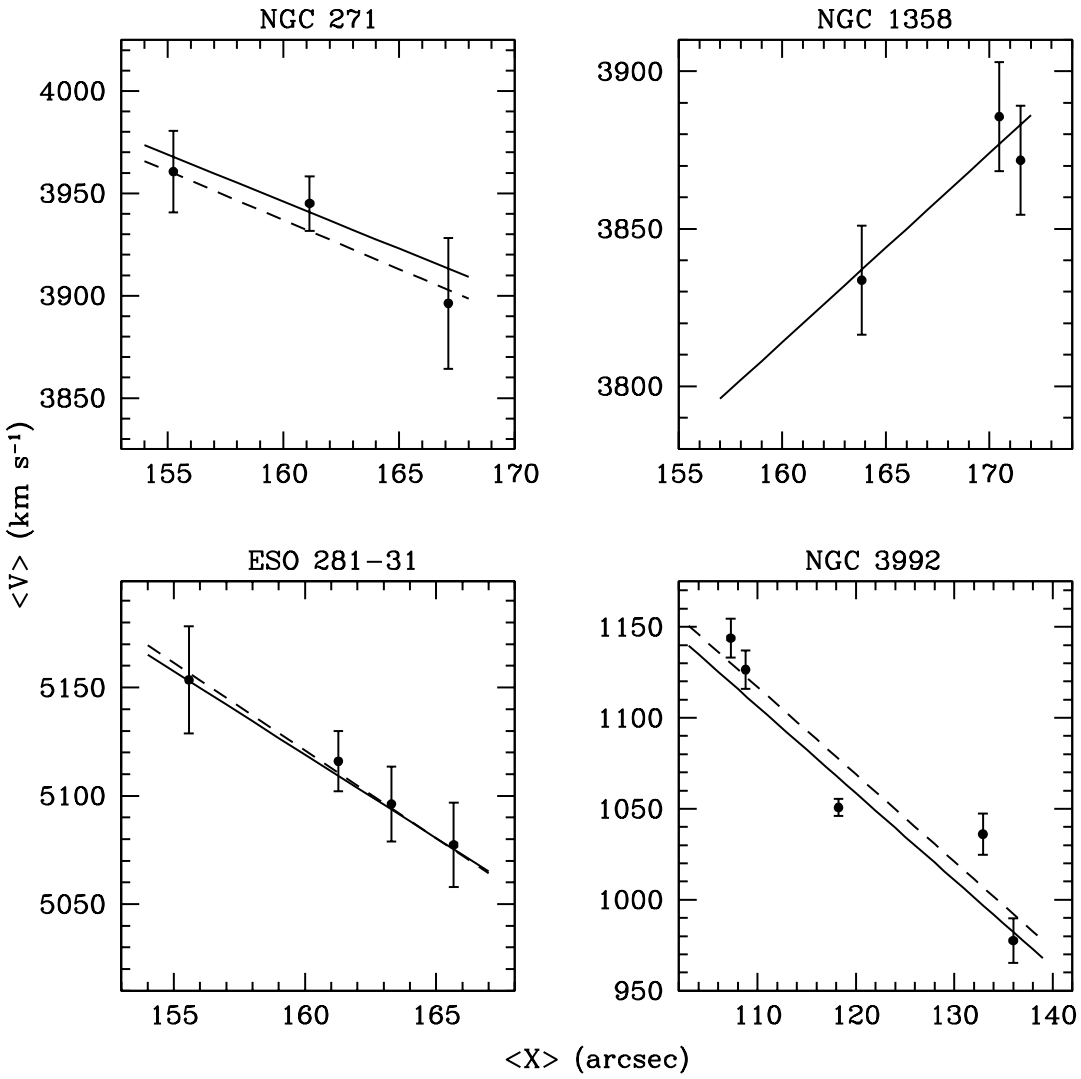

Fig. 2.— The derived mean line-of-sight velocities versus the luminosity centroids for all slits in each of the four galaxies in the sample. The slopes of the linear fits (solid lines) are a measure of $\Omega_p \sin i$ in each galaxy. The dashed lines show the slopes derived from individual exposures rather than from the combined spectra at each slit location (see text).

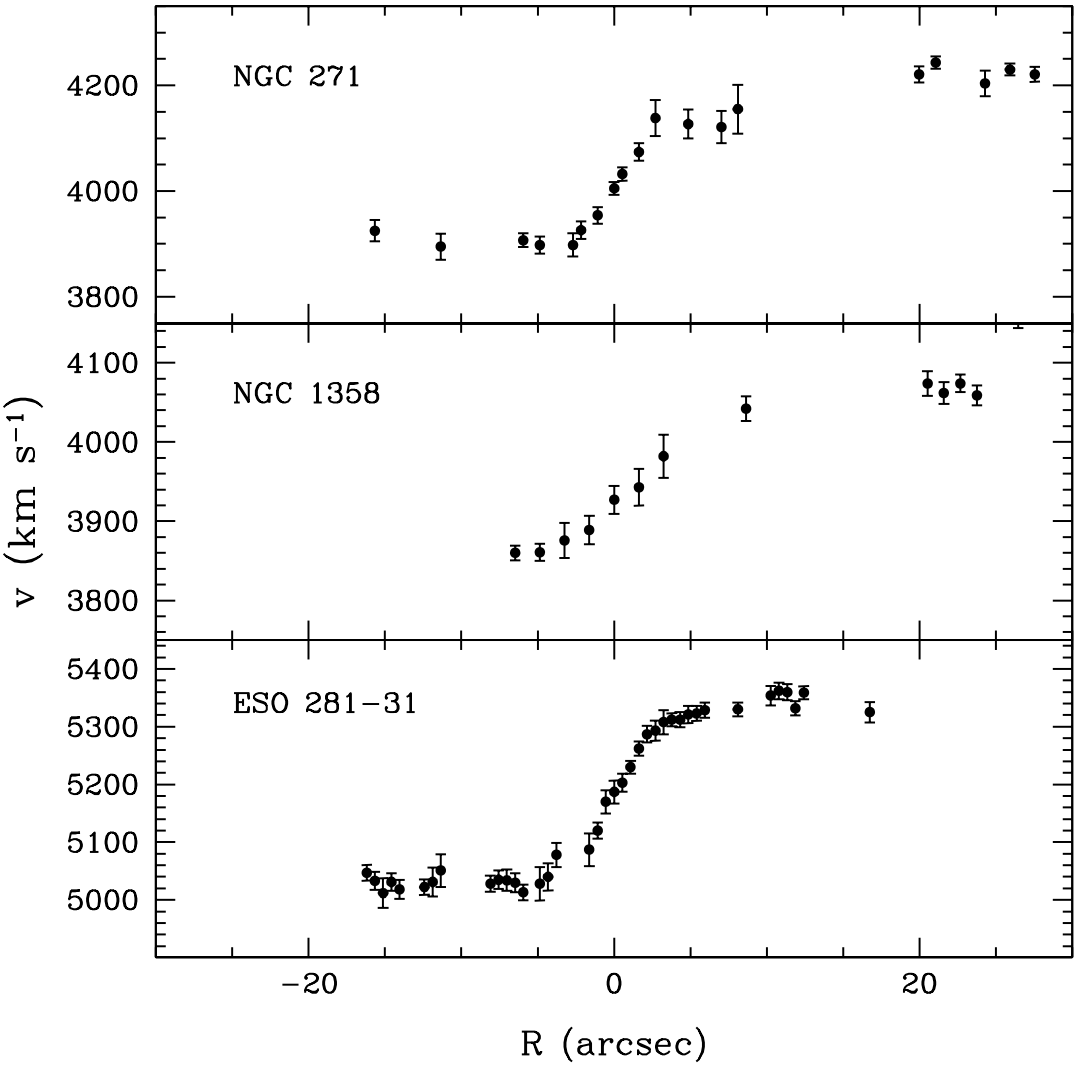

Fig. 3.— The stellar line-of-sight velocities derived using cross-correlation for the three galaxies in our sample for which reliable estimates of the rotation curves were not previously available.

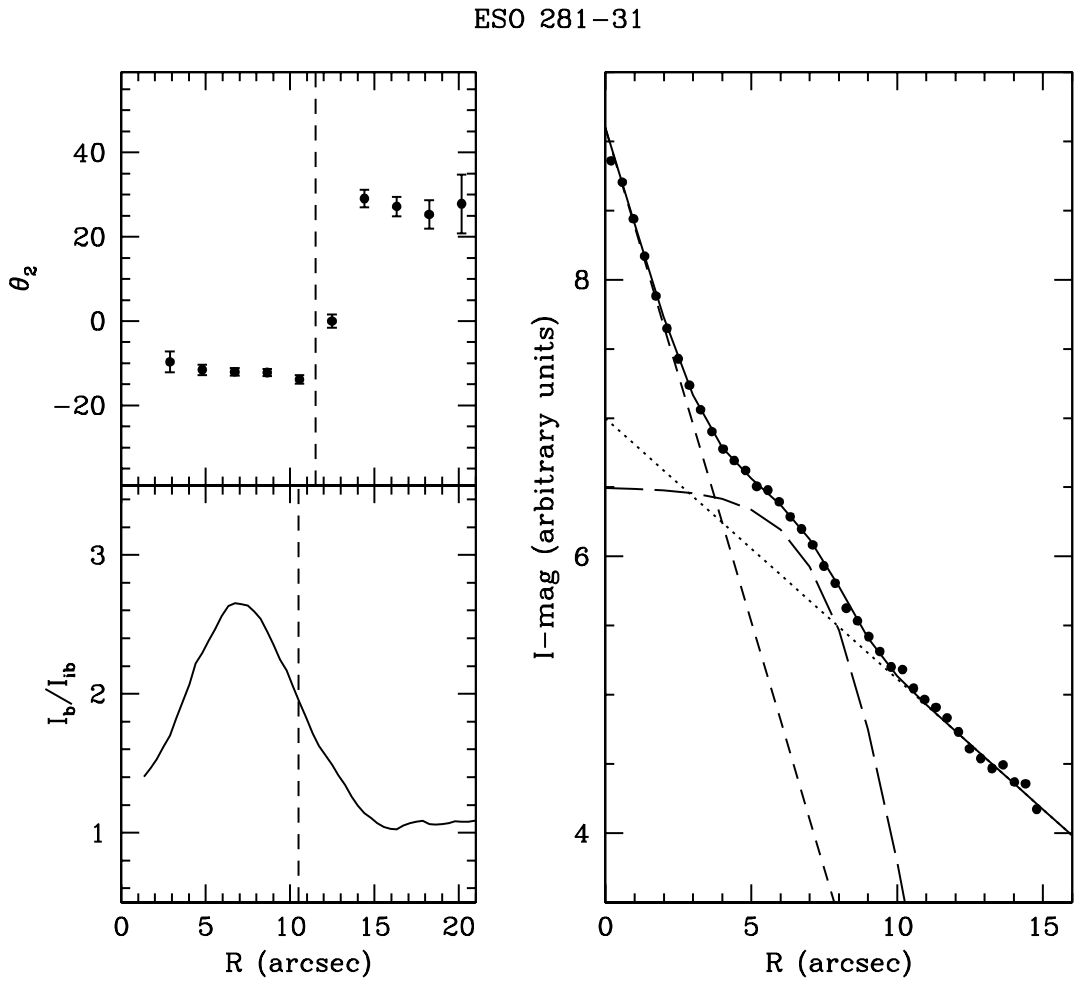

Fig. 4.— Different estimates of the length of the bar in ESO 281-31. The top left panel shows an estimate based on the method of Debattista & Sellwood (2000): along the bar, the phase of the $m = 2$ component of a Fourier decomposition of the (deprojected) surface brightness is constant. In the bottom left panel the bar length is estimated from the ratio of bar/interbar intensities (see text and Aguerri et al. 2000). The dashed line indicates the location where this ratio is consistent with the end of the bar (see text). The panel on the right shows a fit to the surface brightness profile along the bar major axis. Both the bulge (short dash) and the disk (dotted) are assumed to be exponential. The bar component (long dash) is parametrised using the flat-type profile of Prieto et al. (2001).

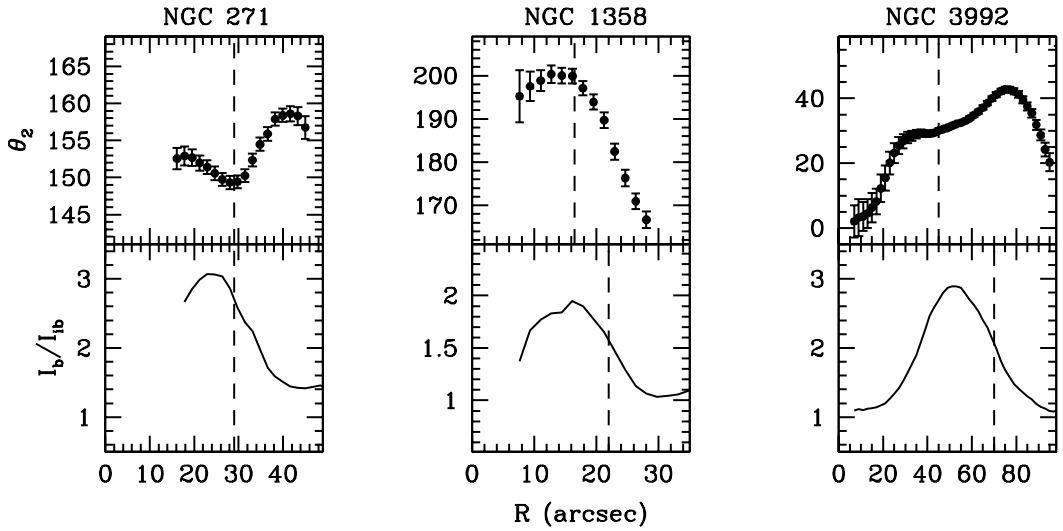

Fig. 5.— Estimates of the bar semi-major axis length in the remaining three galaxies of the sample. The bar lengths are determined using the same Fourier decompositions techniques as in Fig. 4. However, the photometry for these three galaxies is of lower quality than the ESO 281-31 data, and reliable bulge/disk/bar component fits to the surface brightness profiles could not be obtained. In NGC 271 and NGC 1358 the images are over exposed in the centers. These regions were therefore excluded from the analysis.

Table 1. The barred galaxy sample

Galaxy	Type	Redshift (km s^{-1})	PA_{disk}	PA_{bar}	Inclination
NGC 271	SBab	4129	130	178	36 [a)]
NGC 1358	SB0a	4028	195	130	40 [a)]
ESO 281-31	SB0	3459	110	173	47 [b)]
NGC 3992	SBbc	1048	68	37	57 [c)]

Note. — All velocities are from NED.
a) PAs are derived from DSS images, inclinations are from NED.
b) PAs and inclinations are derived from I band photometry.
c) Data taken from Bottema & Verheijen (2002).

Table 2. Observing log

Galaxy	Slit	T_{exp} (sec)
NGC 271	major axis	900
	NW 16".0	2×1800
	SE 16".0	2×1800
NGC 1358	major axis	900
	NW 10".0	2×1800
ESO 281-31	major axis	900 + 1145
	NW 3".6	2×1800
	NW 8".6	2×1800
	SE 8".6	1800
NGC 3992	major axis	900
	NE 30".0	1200 + 1800
	NE 50".0	2×1800
	SW 30".0	1200 + 1800
	SW 50".0	2×1800

Table 3. Observationally derived parameters

Galaxy	$\Omega_p \sin i$ ($\mathrm{km\,s^{-1}arcsec^{-1}}$)	σ_0 ($\mathrm{km\,s^{-1}}$)	h (arcsec)	$R_{\rm CO}$ (arcsec)	$R_{\rm BAR}$ (arcsec)	$R_{\rm BAR-ALT}$ (arcsec)
NGC 271	4.6 ± 2.5	200 ± 10	15.0 ± 1.0	44^{+30}_{-16}	29 ± 1	28.8
NGC 1358	6.0 ± 2.9	180 ± 10	4.5 ± 1.0	23^{+19}_{-7}	19 ± 3	21.4
ESO 281-31	7.7 ± 3.0	150 ± 10	5.3 ± 1.0	20^{+12}_{-4}	11 ± 1	9.7
NGC 3992	4.8 ± 0.3			45^{+3}_{-3}	57 ± 12	67.8

Table 4. Results of the TW method

Galaxy	Type	Ω_p ($\mathrm{km\,s^{-1}kpc^{-1}}$)	$\mathcal{R}$
NGC 271	SBab	25 ± 9	$1.5^{+1.0}_{-0.5}$
NGC 1358	SB0a	31 ± 15	$1.2^{+1.0}_{-0.4}$
ESO 281-31	SB0	27 ± 11	$1.8^{+1.1}_{-0.4}$
NGC 3992	SBbc	73 ± 5	$0.8^{+0.2}_{-0.2}$